Am J Transl Res 2026;18(5):3749-3764
www.ajtr.org /ISSN:1943-8141/AJTR0168575

Original Article

Molecular mechanisms of Buyang Huanwu Decoction in improving Diabetic kidney disease based on network pharmacology and experimental validation

Fan Yang[1,2*], Lifei Liu[3*], Yabin Gao[4*], Xiaoyun Zhang[1], Shengkai Ma[1], Yajing Zhang[5]

[1]College of Integrative Medicine, Hebei University of Chinese Medicine, Shijiazhuang, Hebei, China; [2]Institute of Integrative Medicine, Hebei University of Chinese Medicine, Shijiazhuang, Hebei, China; [3]Chinese Medicine Clinical Skills Center, Hebei University of Chinese Medicine, Shijiazhuang, Hebei, China; [4]First Affiliated Hospital of Henan University of Chinese Medicine, Zhengzhou, Henan, China; [5]College of Traditional Chinese Pharmacy, Hebei University of Chinese Medicine, Shijiazhuang, Hebei, China. [*]Equal contributors.

Received September 4, 2025; Accepted March 20, 2026; Epub May 15, 2026; Published May 30, 2026

Abstract: Objectives: In Chinese medicine, Buyang Huanwu Decoction (BHD) has shown efficacy in improving renal function. Nevertheless, its specific pharmacological mechanisms in treating diabetic kidney disease (DKD) have not yet been fully elucidated. Methods: In this study, the active ingredients of BHD were first identified using the Traditional Chinese Medicine Systems Pharmacology (TCMSP) database, with their potential targets predicted via SwissTargetPrediction and confirmed in TCMSP. DKD-related targets were obtained from the GeneCards and DisGeNET databases. A protein-protein interaction (PPI) network was then constructed with the shared targets using the STRING database. Functional annotation was performed through Gene Ontology (GO) analysis on Metascape, while pathway enrichment analysis was conducted using the Kyoto Encyclopedia of Genes and Genomes (KEGG) via the ClueGO plugin in Cytoscape. Finally, in vivo experiments were performed to validate the mechanisms of BHD. Results: A total of 634 active ingredients were identified in BHD. Among them, 222 corresponded to potential drug targets, and 3,665 disease targets related to DKD were obtained. Based on their intersection, a pharmacological network comprising 156 genes was constructed. Sixteen active ingredients were found to be involved in alleviating renal injury in DKD. GO and KEGG enrichment analyses revealed that the effects of BHD are primarily mediated through pathways related to inflammatory responses, lipid metabolism, and anti-oxidation, including the IL-17 and TNF signaling pathways. Animal experiments further confirmed that BHD alleviates renal fibrosis by inhibiting oxidative stress and inflammation, mechanisms that involve the Nrf2/HO-1 and NF-κB signaling pathways. Conclusions: BHD ameliorates DKD primarily through antioxidative, anti-inflammatory, and anti-fibrotic mechanisms, ultimately reducing proteinuria and preserving renal function.

Keywords: Diabetic kidney disease, Buyang Huanwu Decoction, network pharmacology, oxidative stress, inflammation

Introduction

Diabetic kidney disease (DKD) is a common microvascular complication of diabetes mellitus, which is a main cause of death in diabetic patients [1]. The early clinical features of DKD are microalbuminuria, which gradually develops into severe proteinuria accompanied by a decrease in glomerular filtration rate (GFR). The pathological and development mechanism of DKD are complex, which involves metabolic dysfunction, chronic high blood glucose, hemorheology anomalies, and hemodynamic changes etc. Oxidative stress (OS) and inflammation are important factors, which led to the pathological development of DKD [2-4]. Multiple studies have shown that hyperglycemia can induce renal tissue damage to produce various inflammatory factors and growth factors, and further lead to OS. Meanwhile, OS can promote the release of inflammatory factors and aggravate renal damage [5, 6]. The positive feedback regulation between OS and inflammation aggravates the pathological process of DKD. Therefore, OS is considered the pathogenic basis of DKD.

https://doi.org/10.62347/UROV7218

Current therapeutic strategies for DKD primarily focus on glycemic and blood pressure control, dietary protein restriction, lipid-lowering therapy, and modulation of the renin-angiotensin system [7, 8]. Although these pharmacological interventions are effective to some extent, they are often accompanied by adverse effects, including hypoglycemia, peripheral edema, gastrointestinal reactions, and metabolic acidosis. Therefore, the identification of safe and effective alternative or complementary therapeutic approaches for the prevention and treatment of DKD remains of considerable clinical importance [9]. Accumulating experimental and clinical evidence suggests that Chinese medicinal formulas (CMFs), as well as their bioactive constituents, represent a relatively safe and holistic therapeutic system that has been practiced for thousands of years [10]. From the perspective of traditional Chinese medicine (TCM), qi deficiency and blood stasis obstructing the renal collaterals are recognized as central pathogenetic mechanisms of DKD, a concept that has gained broad acceptance within the TCM academic community [11]. BHD, a classical CMF composed of seven medicinal herbs, is traditionally prescribed to invigorate qi and promote blood circulation. Previous studies have demonstrated that BHD exerts multiple pharmacological effects, including vasodilation, improvement of microcirculation, anti-inflammatory and antioxidative activities, as well as protection of vascular endothelial function [12, 13]. Moreover, clinical studies indicate that BHD can ameliorate lipid metabolism disorders, reduce urinary protein excretion, and significantly improve renal function in patients with DKD [14-16]. Nevertheless, the molecular mechanisms underlying the renoprotective effects of BHD in DKD remain incompletely elucidated.

In the present study, a network pharmacology approach was employed to elucidate the potential mechanisms underlying the therapeutic effects of BHD in DKD. Guided by the network pharmacology findings, in vivo experiments were subsequently conducted to validate the predicted pharmacological effects and molecular mechanisms of BHD. The in vivo results demonstrated that BHD attenuated renal fibrosis and preserved renal function primarily through the suppression of oxidative stress and inflammatory responses. Collectively, these findings provide mechanistic insights into the renoprotective effects of BHD and suggest a promising therapeutic strategy for the clinical management of DKD.

Materials and methods

The composition and dosage of Chinese herbal medicine in BHD

BHD consists of seven herbal granule components: Huangqi (Astragalus mongholicus; Batch No. 012263), Chuanxiong (Ligusticum wallichii; Batch No. 8122561), Honghua (Carthami Flos; Batch No. 101149), Taoren (Persicae Semen; Batch No. 0096363), Dilong (Pheretima aspergillum; Batch No. 7125701), Danggui (Angelica sinensis; Batch No. 0093103), and Chishao (Paeoniae Radix Rubra; Batch No. 0113103). All the TCM granules were obtained from Guangdong Yifang Pharmaceutical Co., Ltd.

Experimental reagents

Microalbumin Assay Kit (mALB), malondialdehyde (MDA), and superoxide dismutase (SOD) (batch No H127-1-2, A003-1-2, A001-3-2) were purchased from Nanjing Jiancheng Bioengineering Research Institute. Fasting blood glucose (FBG), total cholesterol (TC), triglyceride (TG), blood urea nitrogen (BUN), and creatinine (Scr) kit were purchased from Beckman Coulter Experimental System Limited Company (batch No AUZ3765, AUZ3625, AUZ3592, AUZ3611, AUZ3562). Servicebio® RT First Strand cDNA Synthesis Kit, 2×SYBR Green qPCR Master Mix (High ROX), Anti-NF-kB p65 Rabbit pAb, Anti-IKBα pAb, Anti-collagens III Rabbit pAb, Anti-HO-1 Rabbit pAb, Anti-TGF-β1 Rabbit pAb, HRP conjugated Goat Anti-Rabbit IgG, and Anti-Histone H3 Rabbit pAb (batch No G3330, G3321, GB11997, GB111509, GB111364, GB111629, GB12104, GB111876, GB23303, GB11102) were purchased from Wuhan Servicebio Technology Co., Ltd. Anti-Nrf2 Rabbit pAb, Anti-NQO1 Rabbit pAb (batch No 16396-1-AP, 67240-1-Ig) were purchased from Proteintech Co., Ltd. Anti-TNF-α antibody, Anti-IL-1β antibody, Anti-P62 antibody, Anti-Beclin1 antibody, Anti-LC3B antibody (batch No ab6671, ab9722, ab109012, ab62557, ab192890) was purchased from Abcam. Rabbit Anti-phospho-IκB alpha antibody (batch No bs2513R) was purchased from Beijing Biosynthesis Biotechnology Co., Ltd. 8-hydroxy-2-deoxyguanosine (8-OH-dG) As-

say Kit (batch No F02165) was purchased from Shanghai Xitang Biotechnology Co., Ltd. Anti-β-actin antibody, BeyoECL Plus, RIPA Lysis Buffer, Periodic Acid-Schiff Staining Kit, Hematoxylin and Eosin Staining Kit, Enhanced BCA Protein Assay Kit (batch No AF0003, P0018S, P0013B, C0142M, C0105S, P0009) were purchased from Beyotime Biotechnology Co., Ltd.

Interaction network of BHD constituents and DKD target genes

The bioactive components of BHD were retrieved from the Traditional Chinese Medicine Systems Pharmacology Database and Analysis Platform (TCMSP; https://old.tcmsp-e.com/index.php). Compounds meeting the criteria of oral bioavailability (OB) ≥ 30% and drug-likeness (DL) ≥ 0.18 were considered as candidate active ingredients. Active components of Dilong were additionally collected from the BATMAN-TCM database (http://bionet.ncpsb.org.cn/batman-tcm/) [17]. Potential targets of the identified active compounds were obtained from TCMSP and the SwissTargetPrediction database(http://www.swisstargetprediction.ch/).DKD-related targets were collected from the DrugBank database (https://go.drugbank.com/targets, updated on 16 August 2022), GeneCards (https://www.genecards.org/, updated on 10 August 2022), and the Therapeutic Target Database (TTD; https://www.genecards.org/, updated on 16 August 2022). All target proteins were standardized to their corresponding gene symbols using the UniProt database (https://www.uniprot.org/, updated on 16 August 2022). Overlapping targets between BHD-related targets and DKD-associated targets were identified using the Venn diagram tool VENNY 2.1 (https://bioinfogp.cnb.csic.es/tools/venny/, updated on 16 August 2022) [18]. Protein-protein interaction (PPI) networks were constructed using the STRING database, with the species restricted to Homo sapiens and a confidence score threshold set at > 0.7. The resulting PPI network data were imported into Cytoscape software (version 3.9.1; Boston, MA, USA; updated on 16 August 2022) to identify potential core targets associated with DKD [19]. Furthermore, a herb-compound-target network was constructed using Cytoscape 3.9.1 to visualize the interactions between the active components of BHD and their predicted targets [17]. Gene Ontology (GO) functional annotation and Kyoto Encyclopedia of Genes and Genomes (KEGG) pathway enrichment analyses were performed to explore the biological functions and signaling pathways associated with the identified target genes, with results generated using R packages [20].

Animal models and treatment protocols

A total of 48 male Sprague-Dawley (SD) rats (specific pathogen-free grade; 4-5 weeks old; body weight 70 ± 10 g) were obtained from Beijing Vital River Laboratory Animal Technology Co., Ltd. (Beijing, China; License No. SCXK (Beijing) 2023-0151). After one week of acclimatization, the rats were randomly assigned to a control group (C group, n = 10) and a diabetes model group (n = 30). Rats in the control group were fed a standard laboratory chow diet, whereas rats in the diabetic group were fed a high-fat diet (HFD; protein 24.2%, fat 25.4%, carbohydrate 42.1%; Beijing Vital River Laboratory Animal Technology Co., Ltd.) for six weeks. Subsequently, HFD-fed rats were intraperitoneally injected with low-dose streptozotocin (STZ; 35 mg/kg, dissolved in 0.1 mmol/L citrate buffer) to induce diabetes. STZ was administered once daily for three consecutive days, and rats were fasted for 12 h prior to each injection [21]. Rats in the control group received intraperitoneal injections of an equal volume of 0.1 mmol/L citrate buffer for three consecutive days. A sustained elevation in fasting blood glucose levels (≥ 16.7 mmol/L) was considered indicative of successful diabetes model establishment. Six rats died during or after STZ administration. The remaining 24 diabetic rats were randomly allocated to the diabetes mellitus group (DM group, n = 8), BHD treatment group (BHD group, n = 8), and irbesartan treatment group (Irbesartan group, n = 8).

The dosage of BHD was calculated according to Research Methods in Pharmacology of Chinese Materia Medica. Rats in the BHD group received BHD at a dose of 9.5 g/kg, while rats in the Irbesartan group were administered irbesartan at a dose of 13.5 mg/kg. Rats in the control and DM groups received an equivalent volume of normal saline via intragastric administration. All treatments were administered once daily by oral gavage for 12 consecutive

Table 1. Primer sequences for qRT-PCR analysis

Gene	Forward primer (5'-3')	Length of product (bp)
GAPDH	Fwd CTGGAGAAACCTGCCAAGTATG	138
	Rev GGTGGAAGAATGGGAGTTGCT	
IL-1β	Fwd CTCACAGCAGCATCTCGACAAGAG	95
	Rev TCCACGGGCAAGACATAGGTAGC	
TNF-α	Fwd CCAGGTTCTCTTCAAGGGACAA	80
	Rev GGTATGAAATGGCAAATCGGCT	
HO-1	Fwd CAGCATGTCCCAGGATTTGTC	145
	Rev CCTGACCCTTCTGAAAGTTCCTC	
NQO1	Fwd AGGCTGCTGTGGAGGCTCTG	120
	Rev GCTCCCCTGTGATGTCGTTTCTG	

weeks. All animal procedures were approved by the Animal Experimental Ethics Committee of Hebei University of Chinese Medicine (Approval No. DWLL202203117).

Specimen collection

At the end of the experimental period, rats were individually housed in metabolic cages for urine collection. Urine samples were centrifuged at 4,000×g for 15 min at 4°C, and the supernatants were stored at -80°C for subsequent analyses. Following a 12-h fasting period, rats were anesthetized with 3% isoflurane, and blood samples were collected from the femoral artery. Serum was obtained by centrifugation at 4,000×g for 10 min at 4°C. All animals were euthanized by cervical dislocation. Kidneys were immediately excised, and the renal capsules were carefully removed. Each kidney was divided into two portions: one portion was fixed in 4% paraformaldehyde for histopathological and immunohistochemical analyses, while the other portion was snap-frozen and stored at -80°C for subsequent protein expression analysis.

Metabolic and biochemical parameter analysis

The mALB levels were measured using a commercial mALB assay kit, and results were expressed as milligrams per 24 hours. Blood samples were centrifuged at 4°C for 10 min to obtain serum, which was subsequently used to determine levels of BUN, Scr, CHO, and TG using a Hitachi automatic biochemical analyzer (7600-020, Hitachi, Tokyo, Japan). Renal tissue was homogenized, and the contents of MDA and 8-OHdG, as well as SOD activity, were measured using commercially available assay kits according to the manufacturers' instructions.

Quantitative Real-time Polymerase Chain Reaction (qRT-PCR) assay

Total RNA was extracted from kidney tissues using TRIzol reagent, and RNA concentrations were determined with a NanoDrop 2000C spectrophotometer (Thermo Scientific, Wilmington, USA). The isolated RNA was subsequently reverse-transcribed into complementary DNA (cDNA) using the Servicebio® RT First Strand cDNA Synthesis Kit. The qRT-PCR was performed on the cDNA using 2×SYBR Green qPCR Master Mix (High ROX). Relative mRNA expression levels were calculated using the $2^{-\Delta\Delta Ct}$ method, with GAPDH serving as the internal reference gene. Primer sequences are listed in **Table 1**.

Western blot

Renal tissues (100 mg per sample) were washed twice with ice-cold phosphate-buffered saline (PBS) and lysed in 980 μL of ice-cold modified RIPA buffer supplemented with HALT protease and phosphatase inhibitor cocktail. Lysates were incubated on ice for 10 min, followed by centrifugation at 10,000 rpm for 10 min at 4°C to collect the supernatants. Protein concentrations were determined using the bicinchoninic acid (BCA) assay. For Western blot analysis, equal amounts of protein were separated by SDS-PAGE and transferred onto polyvinylidene difluoride membranes. Membranes were blocked with 5% skim milk in Tris-buffered saline containing 0.1% Tween-20 (TBST) at room temperature for 1 h, and then incubated overnight at 4°C with the following primary antibodies: Nrf2 (1:500), NQO1 (1:800), HO-1 (1:800), NF-κB (1:800), IκBα (1:800), p-IκBα (1:600), IL-1β (1:1000), TNF-α (1:800), P62 (1:800), Beclin1 (1:800), LC3B (1:800), Histone (1:1000), and β-actin (1:1000). After washing, membranes were incubated with horseradish peroxidase-conjugated secondary antibodies at room temperature for 1 h. Protein signals were visualized using enhanced chemiluminescence (ECL) detection kits.

Histological analysis and immunohistochemistry staining

Paraffin-embedded kidney tissues were sectioned at 2 μm thickness. Sections were deparaffinized in xylene, rehydrated through a graded ethanol series, and subjected to antigen retrieval using citric acid solution. Endogenous peroxidase activity was blocked by incubating sections with 3% H_2O_2 in the dark for 25 min, followed by blocking with 3% bovine serum albumin for 30 min. Sections were then incubated overnight at 4°C with primary antibodies against Col-III (1:300) and TGF-β1 (1:200), followed by incubation with horseradish peroxidase-conjugated goat anti-rabbit IgG for 50 min at room temperature. Signals were developed using 3,3'-diaminobenzidine, and sections were counterstained with hematoxylin. Images were captured in a blinded manner and analyzed using Image-Pro Plus 6.0 software (Media Cybernetics, USA).

For immunofluorescence analysis, kidney tissue sections were deparaffinized, rehydrated, and subjected to antigen retrieval as described above. Sections were incubated overnight at 4°C with primary antibody against NF-κB (1:200), followed by incubation with Alexa Fluor® 594-conjugated goat anti-rabbit IgG secondary antibody for 30 min at room temperature. Nuclei were counterstained with 4',6-diamidino-2-phenylindole (DAPI), and images were acquired using an Olympus IX71 fluorescence microscope (Olympus, Japan).

Statistical analysis

All data were analyzed using SPSS software (version 26.0; IBM, Chicago, IL, USA) and are presented as mean ± standard deviation (SD). Graphs were generated using GraphPad Prism software (version 5.02; GraphPad Software Inc., San Diego, CA, USA). Comparisons between two groups were performed using the unpaired Student's t-test, while comparisons among multiple groups were conducted using one-way analysis of variance (ANOVA) followed by appropriate post hoc tests. Differences were considered statistically significant at $P < 0.05$.

Results

The network pharmacology analysis of BHD

Using the thresholds of OB ≥ 30% and DL ≥ 0.18, a total of 60 active ingredients from the seven constituent herbs of BHD were retrieved from TCMSP, along with four additional active compounds from Dilong identified via BATMAN-TCM. In total, 634 active ingredients were identified in BHD (Table S1). A total of 222 corresponding protein targets were obtained from the SwissTargetPrediction and PharmMapper databases. Meanwhile, 3,665 DKD-associated targets were collected from DrugBank, OMIM, TTD, and PharmGKB databases (Table S2). Intersection analysis between compound-related targets and disease-associated genes, performed using the VENNY 2.1 online tool, yielded 156 overlapping targets (**Figure 1A**).

PPI network was constructed by importing these 156 intersecting targets into the STRING database (confidence score > 0.7) (**Figure 1B**), and the network was visualized in Cytoscape 3.9.1. The resulting PPI network consisted of 114 nodes and 1,117 edges (**Figure 1D**), where each node represents a target gene, and edges indicate interactions. Node color reflects degree, ranging from yellow (lowest) to purple (highest). Nineteen key targets were identified using a median degree threshold ≥ 30, and the 10 most centrally located nodes - TP53, AKT1, JUN, TNF, CASP3, EGFR, MYC, CTNNB1, MAPK1, and RELA - were considered potential core anti-DKD targets of BHD (**Figure 1C**; Table S3).

To further explore the relationship between active compounds and disease targets, a drug - target network was constructed consisting of 63 active compounds and 156 disease targets, comprising 271 nodes and 541 edges (**Figure 1E**). In this network, nodes represent compounds or targets, and edges represent interactions. The degree of a node reflects the number of interactions, with higher-degree nodes indicating greater involvement in network regulation. Sixteen compounds exhibited degrees greater than 9, including quercetin (MOL000098, degree = 106), luteolin (MOL000006, degree = 47), kaempferol (MOL000422, degree = 44), baicalein (MOL002714, degree = 28), formononetin (MOL000392, degree = 22), and isorhamnetin (MOL000354, degree = 22), suggesting that these compounds may play central roles in the anti-DKD effects of BHD (Table S4).

The functional analysis of biological information

To investigate the potential pharmacological mechanisms of BHD in DKD, GO and KEGG

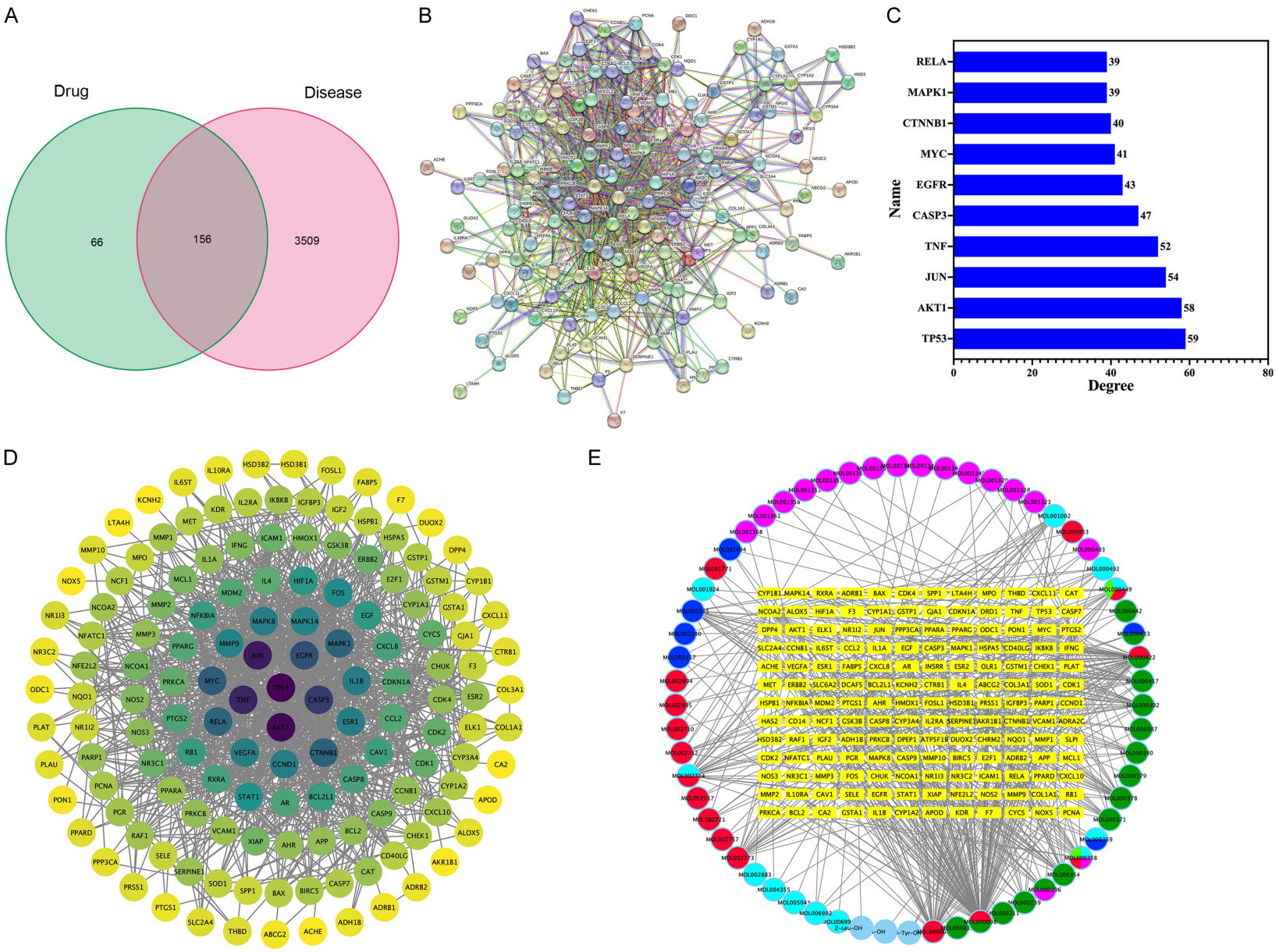
A
Drug
Disease
66
156
3509
B
C
RELA 39
MAPK1 39
CTNNB1 40
MYC 41
EGFR 43
CASP3 47
TNF 52
JUN 54
AKT1 58
TP53 59
Name
0
20
40
60
80
Degree
D
E

Figure 1. The Network pharmacological analysis of DKD improved by BHD. A. Venn diagram between disease-related genes and targets of active chemical ingredients. B. A PPI network was constructed using STRING database. C. 10 potential core targets with a degree higher than 39. D. Results of STRING is visualized and analyzed by Cytoscape software 3.9.1. E. Network between the 63 active compounds and 156 intersecting targets.

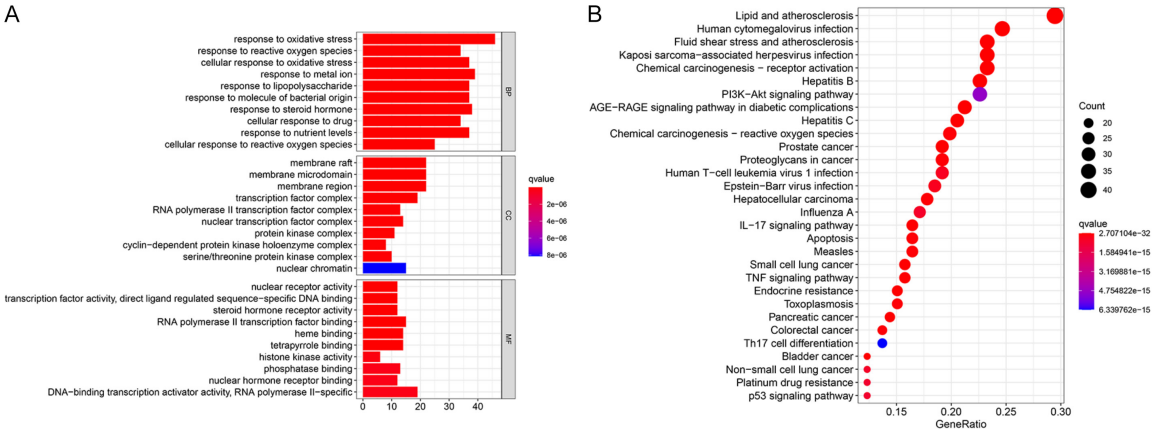

Figure 2. GO and KEGG enrichment analyses. A. GO enrichment analysis of 156 intersecting targets for the treatment of DKD with BHD. B. KEGG enrichment analysis of 156 therapeutic genes for DKD by BHD.

pathway enrichment analyses were performed on the 156 intersecting targets. GO analysis identified 2,390 biological process (BP), 62 cellular component (CC), and 172 molecular function (MF) terms with $P \leq 0.05$. The top 10 significantly enriched terms in each category are presented in a bar plot (**Figure 2A**). BP analysis revealed that target proteins were primarily involved in oxidative stress and responses to reactive oxygen species. CC terms were enriched for transcription factor complexes and nuclear transcription factor complexes. MF analysis indicated that target proteins were associated with RNA polymerase II transcription factor binding, DNA-binding transcription activator activity, and RNA polymerase II-specific activity.

KEGG pathway enrichment analysis identified the top 30 significantly enriched pathways (**Figure 2B**), including IL-17 and TNF signaling pathways. Additional pathways were related to lipid metabolism and oxidative stress responses. Collectively, these GO and KEGG enrichment analyses suggest that the therapeutic effects of BHD in DKD may involve modulation of inflammatory responses, lipid metabolism, and antioxidative processes.

Effects of BHD on metabolic and biochemical parameters

Compared with the C group, DM rats exhibited significant increases in FBG, CHO, TG, BUN, SCr, and mALB levels (**Figure 3A-F**, $P < 0.01$). Treatment with BHD significantly reduced CHO, TG, BUN, SCr, and mALB compared with the DM group (**Figure 3B-F**, $P < 0.01$), whereas FBG levels remained unchanged (**Figure 3A**, $P > 0.05$), indicating that BHD administration did not affect hyperglycemia. In the Irbesartan-treated group, BUN, SCr, and mALB were significantly decreased relative to the DM group (**Figure 3D-F**, $P < 0.01$), while FBG, CHO, and TG levels were not significantly altered (**Figure 3A-C**, $P > 0.05$). Collectively, these results indicate that BHD ameliorates renal dysfunction and dyslipidemia in DKD, without affecting fasting blood glucose levels.

Effects of BHD on renal pathological

Histopathological changes in renal tissues were assessed by HE, PAS, and Masson's trichrome staining. As shown in **Figure 4A**, DM rats exhibited marked kidney injury, including glomerular hypertrophy, extracellular matrix proliferation, thickening of the basement membrane, inflammatory cell infiltration, and localized fibrosis, compared with the C group. Treatment with BHD or Irbesartan markedly attenuated these pathological alterations and reduced inflammatory infiltration. Masson's trichrome staining was used to assess collagen deposition as an indicator of renal fibrosis. The DM group showed significantly increased collagen accumulation relative to the C group (**Figure**

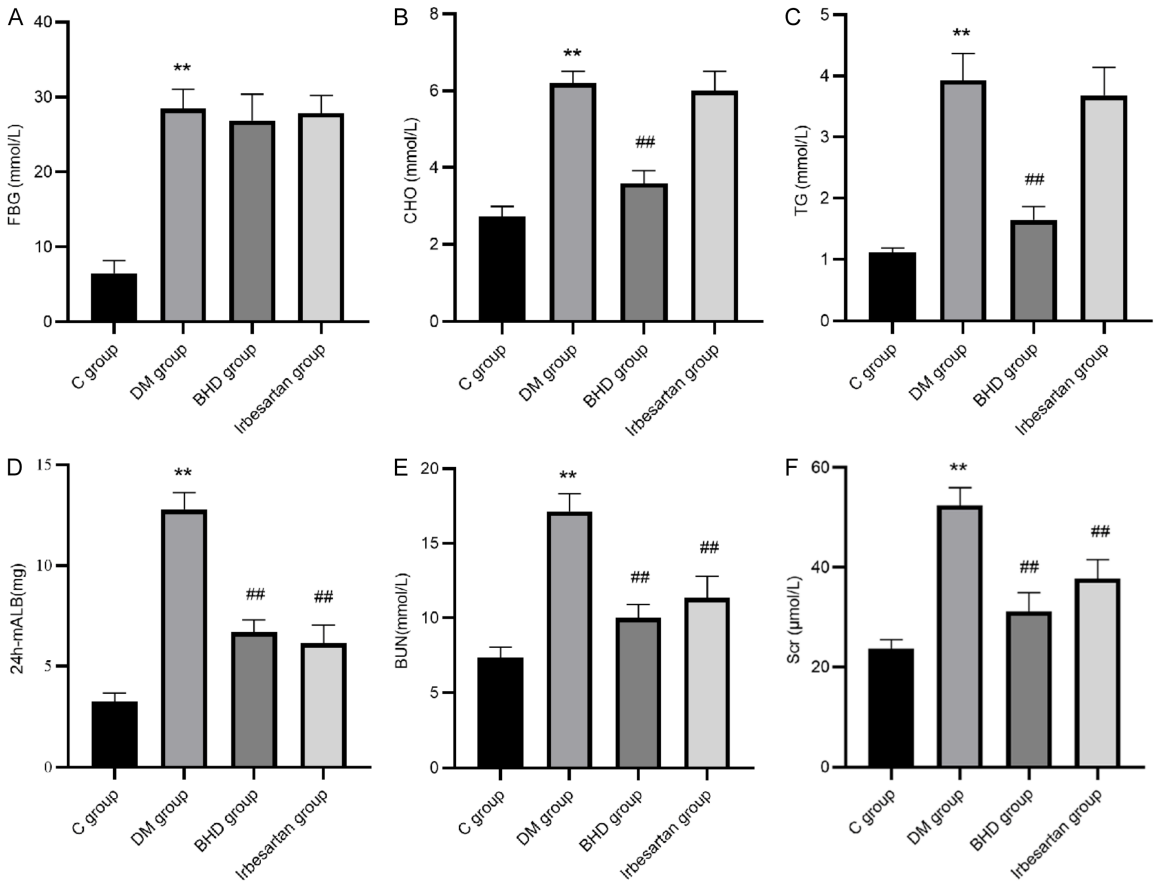

Figure 3. BHD reduces blood lipids and improves kidney function. A. The serum level of FBG. B. The serum level of CHO. C. The serum level of TG. D. The urine level of mALB. E. The urine level of BUN. F. The urine level of Scr. Data are presented as means ± SD (n = 8). $^{**}P < 0.01$ vs. C group. $^{\#\#}P < 0.01$ vs. DM group.

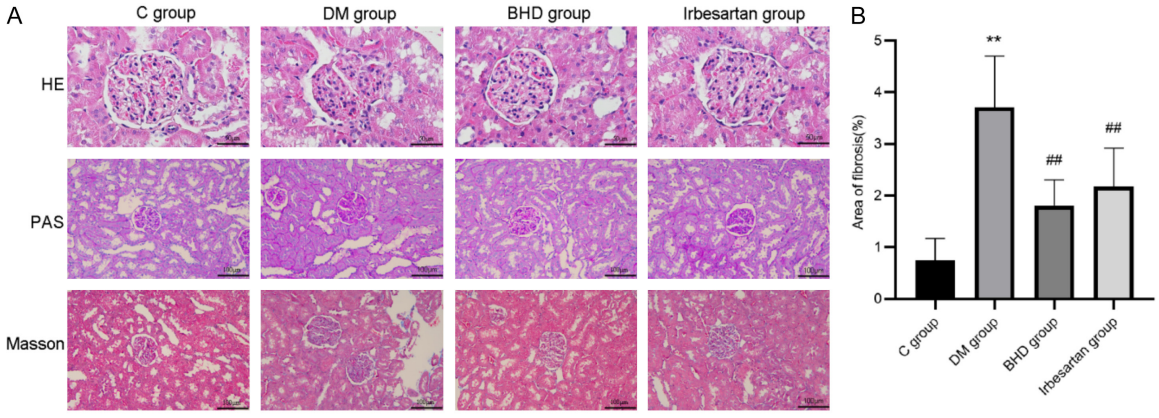

Figure 4. Effects of BHD on renal histopathology of diabetic rats. A. Pathological morphology of renal tissues in each group rats (HE ×400, PAS, Masson ×200). B. Fibrosis area of renal tissues in each group rats. Data are presented as means ± SD (n = 6). $^{**}P < 0.01$ vs. C group; $^{\#\#}P < 0.01$ vs. DM group.

4B, $P < 0.01$). Both BHD and Irbesartan treatments significantly reduced collagen deposition compared with the DM group (**Figure 4B**, $P < 0.01$), indicating their protective effects against renal fibrosis.

The therapeutic effect of BHD on improving OS

OS is recognized as a key contributor to DKD pathogenesis [5], and the Nrf2 signaling pathway plays a central role in regulating the antioxi-

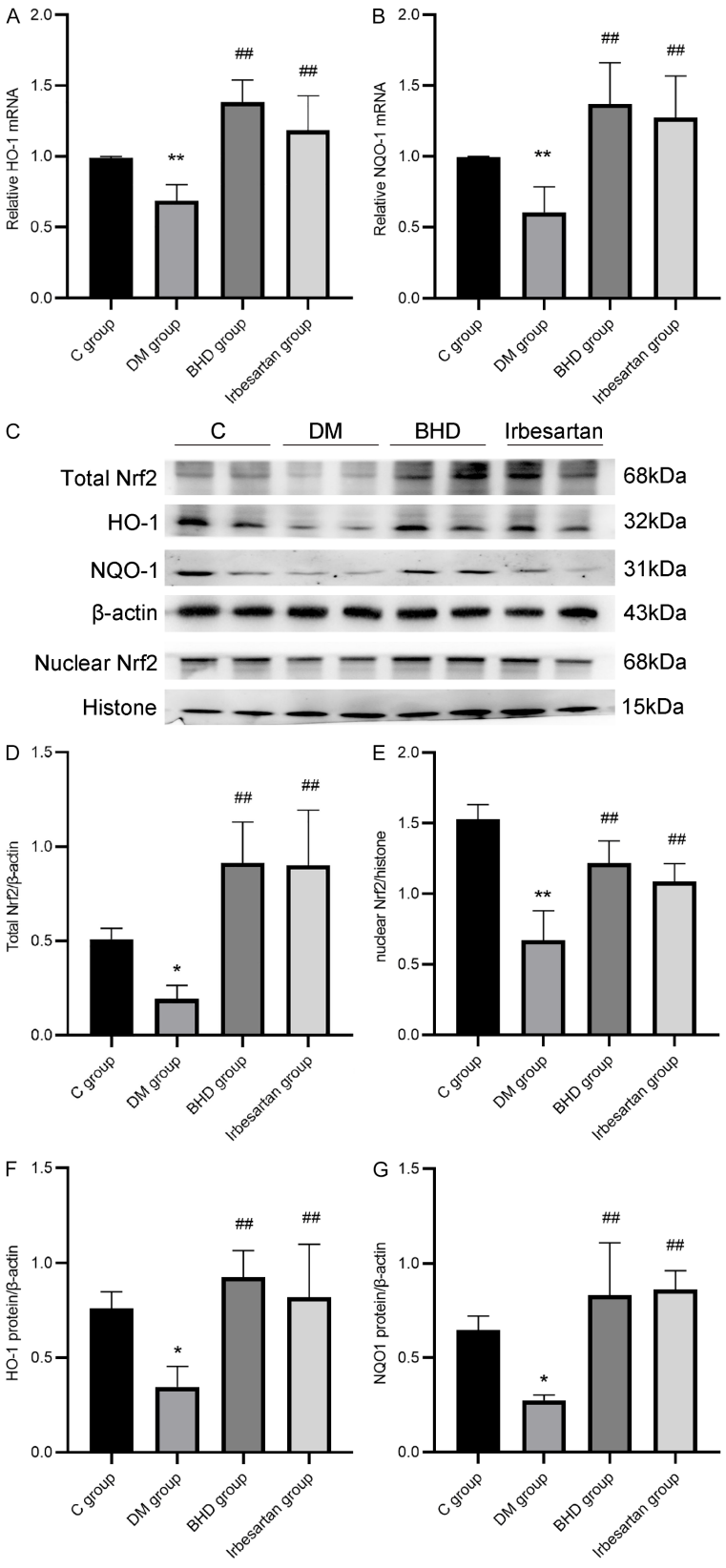

Figure 5. Effects of BDH on the activation of Nrf2 signaling pathways. A. The expressions of HO-1 mRNA were detected by qRT-PCR in rat renal tissues. B. The expressions of NQO1 mRNA were detected by qRT-PCR in rat renal tissues. C. The expressions of Nrf2 pathway activation related proteins in each group rats. D. The quantitative analysis of total Nrf2 protein expression. E. The quantitative analysis of nuclear Nrf2 protein expression. F. The quantitative analysis of total HO-1 protein expression. G. The quantitative analysis of total NQO1 protein expression. Data are presented as means ± SD (n = 3). $^{**}P < 0.01$ vs. C group; $^{\#}P < 0.05$ and $^{\#\#}P < 0.01$ vs. DM group.

dant response by promoting the expression of downstream targets, including HO-1 and NQO1 [22]. To evaluate the antioxidant effects of BHD, the mRNA and protein levels of HO-1 and NQO1 were assessed. qRT-PCR analysis revealed that HO-1 (**Figure 5A**) and NQO1 (**Figure 5B**) mRNA expression was significantly reduced in DM rats compared with controls ($P < 0.01$). Treatment with BHD or Irbesartan markedly increased the mRNA levels of both HO-1 and NQO1 ($P < 0.01$). Consistently, Western blot analysis showed similar trends at the protein level for HO-1 (**Figure 5C**, **5F**) and NQO1 (**Figure 5C**, **5G**).

We further examined Nrf2 localization by assessing cytoplasmic and nuclear protein levels. Compared with C group rats, both cytoplasmic and nuclear Nrf2 expression were significantly decreased in DM rats (**Figures 5D**, **5E**, S1; $P < 0.01$). Administration of BHD or Irbesartan significantly increased both cytoplasmic and nuclear Nrf2 levels (**Figures 5D**, **5E**, S1; $P < 0.01$), indicating that these treatments promote Nrf2 nuclear translocation and activate antioxidant responses in the kidney.

Effects of BHD on anti-inflammatory responses

OS is closely associated with inflammatory responses. To investigate the anti-inflammatory effects of BHD, the expression of inflammation-related factors TNF-α and IL-1β was evaluated. As shown in **Figure 6A**, protein levels of TNF-α (**Figure 6D**, $P < 0.01$) and IL-1β (**Figure 6D**, $P < 0.05$) were markedly elevated in the kidneys of DM rats compared with controls. Treatment with BHD or Irbesartan significantly attenuated these increases (**Figure 6D**). The mRNA expression patterns of TNF-α (**Figure 6C**, $P < 0.05$) and IL-1β (**Figure 6C**, $P < 0.01$) mirrored the protein expression trends across all groups.

Activation of the NF-κB signaling pathway is known to upregulate TNF-α and IL-1β expression [23]. We therefore assessed NF-κB pathway activation in renal tissues. Compared with the C group, DM rats exhibited increased levels of nuclear NF-κB (**Figure 6E**, $P < 0.01$) and p-IκBα (**Figure 6F**, $P < 0.01$), accompanied by decreased cytoplasmic IκBα (**Figure 6F**, $P < 0.01$). BHD treatment significantly reduced p-IκBα and restored IκBα levels relative to DM rats ($P < 0.05$ and $P < 0.01$, respectively). Irbesartan significantly reduced p-IκBα levels but had no effect on IκBα (**Figure 6F**, $P < 0.05$). Both BHD and Irbesartan effectively inhibited total NF-κB expression and its nuclear translocation (**Figure 6A**, **6E**). Consistently, immunofluorescence analysis demonstrated that BHD and Irbesartan markedly suppressed NF-κB nuclear translocation in renal tissues (**Figure 6B**, **6G**, $P < 0.01$).

Effects of BHD on OS and autophagy

Autophagy is closely associated with renal injury in DKD, playing a critical role in clearing protein aggregates and damaged organelles to maintain cellular homeostasis [24]. OS can induce autophagy to remove mitochondria, endoplasmic reticulum, peroxisomes, and oxidatively damaged proteins [25]. Consistent with oxidative injury, DM rats exhibited significantly increased levels of MDA (**Figure 7A**, $P < 0.01$) and 8-OH-dG (**Figure 7C**, $P < 0.01$), along with decreased SOD activity (**Figure 7B**, $P < 0.01$) compared with the C group. Treatment with BHD or Irbesartan significantly reduced MDA and 8-OH-dG levels and restored SOD activity (**Figure 7A-C**, $P < 0.01$), indicating effective attenuation of OS.

To assess autophagy, key markers including P62, Beclin1, and LC3B were measured [26]. Compared with controls, DM rats exhibited increased P62 expression and decreased Beclin1 and LC3B-II/LC3B-I ratios (**Figures 7D-F**, S2, $P < 0.01$), indicating impaired autophagic flux. Intervention with BHD or Irbesartan significantly reversed these changes, decreasing P62 levels and increasing Beclin1 expression and LC3B-II/LC3B-I ratios (**Figures 7D-F**, S2, $P < 0.01$), demonstrating that both treatments effectively activated renal autophagy in DKD rats.

Effects of BHD on fibrosis cytokine levels

Renal fibrosis represents the terminal stage of DKD progression, characterized by excessive extracellular matrix (ECM) deposition. Collagen and fibronectin serve as key fibrotic markers, contributing to glomerulosclerosis and fibrotic remodeling. Transforming growth factor β1 (TGF-β1) is a central profibrotic cytokine that promotes ECM accumulation, including collagen III [27]. Immunohistochemical analysis revealed that collagen III and TGF-β1 levels were significantly elevated in the kidneys of DM rats compared with controls (**Figure 8A-C**, $P < 0.01$). Treatment with BHD or Irbesartan markedly reduced the expression of collagen III and TGF-β1 (**Figure 8A-C**, $P < 0.01$), indicating effective attenuation of renal fibrosis in DKD.

Discussion

DKD is the most prevalent microvascular complication of diabetes mellitus, with its progression involving multiple molecular targets and signaling pathways. Although current clinical interventions can alleviate some symptoms of DKD, the disease frequently progresses to irreversible renal failure. Therefore, identifying novel and effective therapeutic strategies for DKD remains of critical importance. CMFs have demonstrated therapeutic potential across a variety of diseases through multi-target and multi-pathway mechanisms. However, the complex composition of Chinese herbs poses challenges for elucidating their underlying molecular mechanisms. Network pharmacology has emerged as a powerful approach to systematically investigate the pharmacological mechanisms of CMFs in complex diseases. Previous studies have reported that formulas containing Astragalus mongholicus Bunge and Panax no-

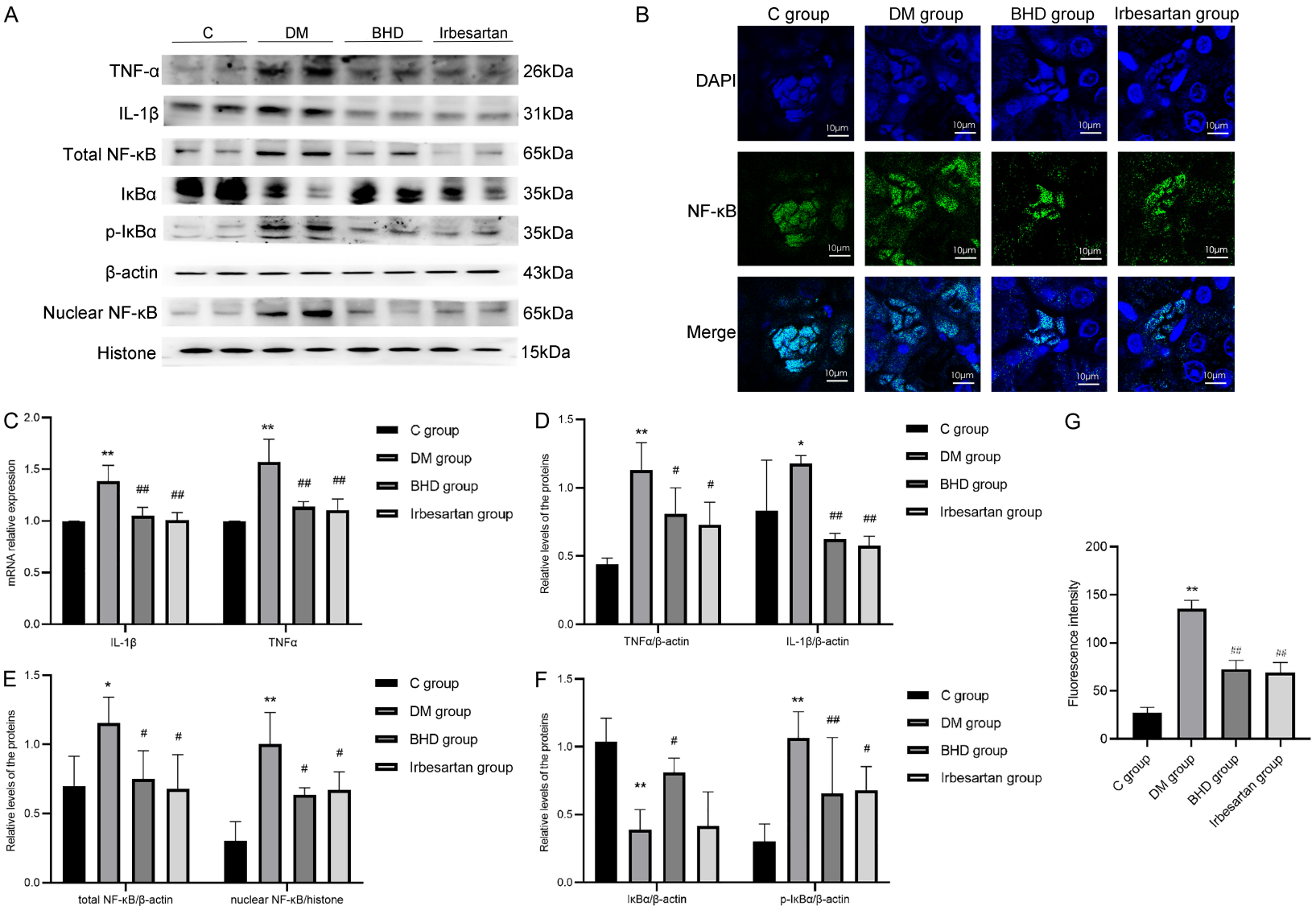

Figure 6. Effects of BDH on the activation of NF-κB signaling pathways. A. Protein expressions of NF-κB pathway activation and related inflammation factors. B. Protein expression of NF-kB nuclear transfer detected by immunofluorescence. C. The mRNA expressions of TNF-α and IL-1β (n = 3). D. Quantitative analysis the protein expressions of TNF-α and IL-1β (n = 3). E. Quantitative analysis the protein expressions of total NF-κB and nuclear NF-κB (n = 3). F. Quantitative analysis the protein expressions of IκBα and p-IκBα (n = 3). G. The fluorescence intensity of NF-κB (n = 6). Data are presented as means ± SD. $^{**}P < 0.01$ vs. C group; $^{\#}P < 0.05$ and $^{\#\#}P < 0.01$ vs. DM group.

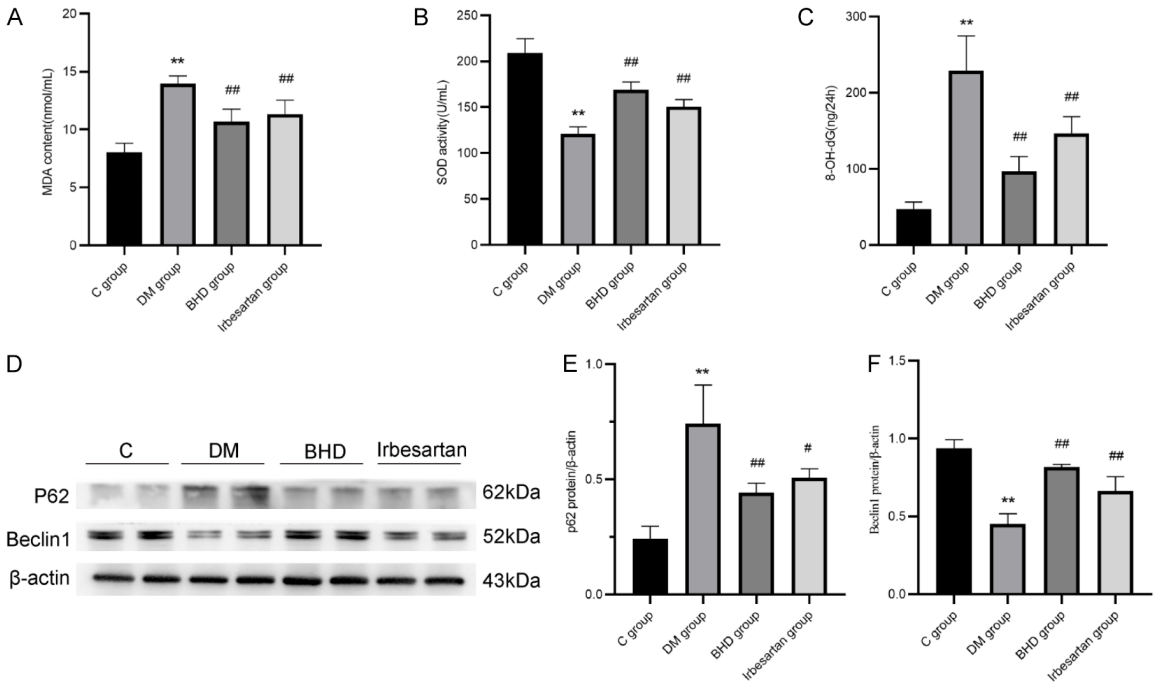

Figure 7. BHD inhibits OS and improves autophagy. A. The levels of MDA. B. The activities of SOD. C. The levels of 8-OH-dG. D. The protein expressions of P62 and Beclin1. E. The quantitative analysis of P62 protein. F. The quantitative analysis of Beclin1 protein. Data are presented as means ± SD (n = 3). $^{**}P < 0.01$ vs. C group; $^{\#}P < 0.05$ and $^{\#\#}P < 0.01$ vs. DM group.

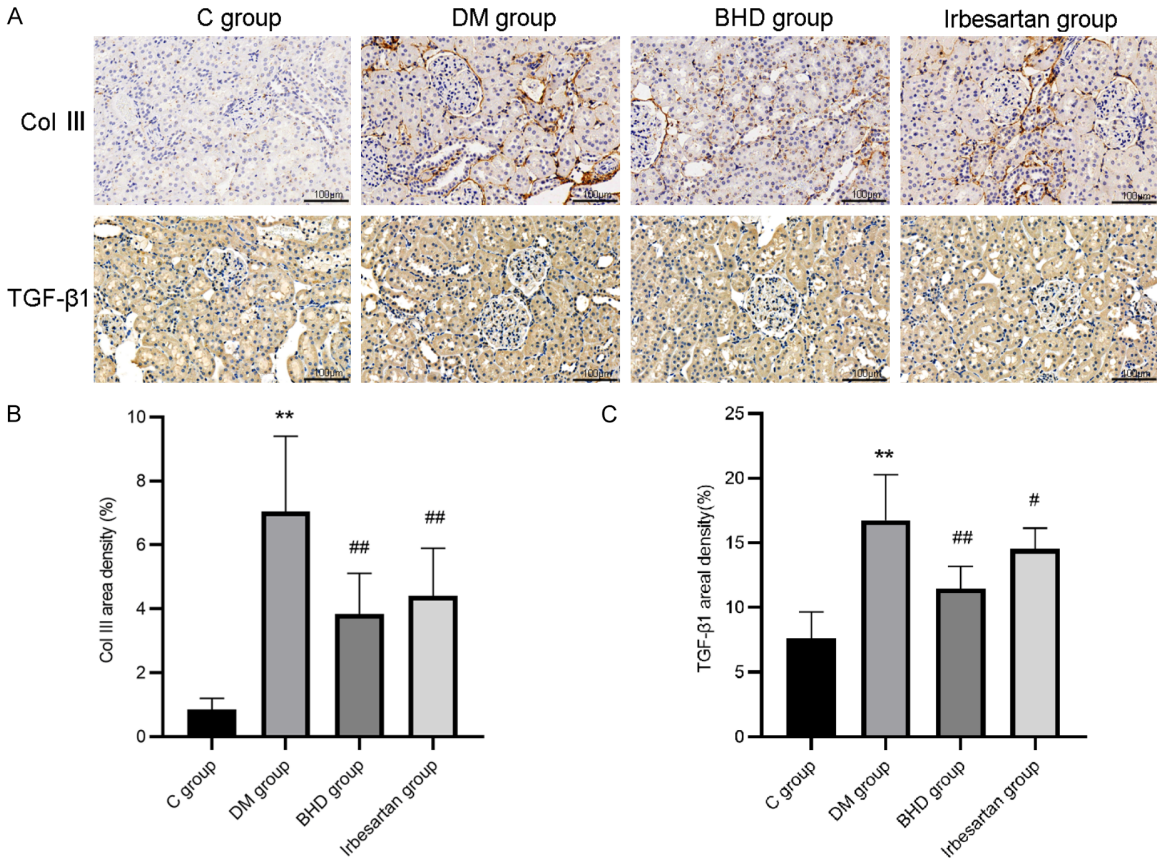

Figure 8. BHD inhibits the expression of collagen III and TGF-β1. A. The immunohistochemistry staining of collagen III and TGF-β1. B. The quantitative analysis of collagen III. C. The quantitative analysis of TGF-β1. Data are presented as means ± SD (n = 6). $^{**}P < 0.01$ vs. C group; $^{\#}P < 0.05$ and $^{\#\#}P < 0.01$ vs. DM group.

toginseng (Burkill) F.H. Chen can ameliorate renal injury in DKD by suppressing mTOR signaling and activating PINK1/Parkin-mediated mitophagy [28], or by inhibiting inflammatory responses [29]. Nevertheless, the potential therapeutic effects and mechanisms of BHD in DKD have not yet been explored.

In this study, network pharmacology was employed to predict the pharmacological mechanisms of BHD in DKD, followed by experimental validation. A total of 634 active ingredients were identified from BHD based on the screening criteria of OB (≥ 30) and DL (≥ 0.18). From these compounds, 222 potential targets were obtained, while 3,665 DKD-associated disease targets were retrieved from multiple databases, yielding 156 intersecting genes. A drug-target network was subsequently constructed, revealing 16 key active ingredients - including quercetin, luteolin, kaempferol, baicalein, formononetin, isorhamnetin, 7-O-methylisomucronulatol, beta-carotene, myricanone, calycosin, ellagic acid, beta-sitosterol, stigmasterol, 3,9-di-O-methylnissolin, (6aR,11aR)-9,10-dimethoxy-6a,11a-dihydro-6H-benzofurano[3,2-c] chromen-3-ol, and jaranol - which may contribute to renal protection in DKD.

Several of these compounds have previously been reported to exert renoprotective effects. Quercetin inhibits glomerular mesangial cell proliferation, mitigating renal injury in DKD, while kaempferol suppresses type IV collagen and TGF-β1 expression and enhances antioxidant defenses to alleviate renal fibrosis [30]. Baicalein and luteolin inhibit renal fibrosis in vitro [31], and baicalin modulates oxidative stress and inflammation via the Nrf2 and MAPK signaling pathways [32]. Furthermore, beta-sitosterol, stigmasterol, quercetin, formononetin, kaempferol, jaranol, and calycosin, as major bioactive constituents of Yishen capsules, exhibit anti-inflammatory and antioxidative effects in the context of diabetes and its complications [33].

The network analysis also highlighted key protein targets involved in these processes. AKT1 is closely associated with systemic inflammation, whereas EGFR and CASP3 contribute to improved microcirculation, free radical scavenging, and suppression of inflammatory mediators. Collectively, these findings suggest that BHD exerts multi-component, multi-target protective effects in DKD, primarily through regulation of oxidative stress, inflammation, and fibrosis.

KEGG pathway enrichment analysis revealed that the majority of significantly enriched pathways were associated with inflammation and oxidative stress responses. Among the top 30 pathways, TNF and IL-17 signaling pathways were closely linked to inflammatory regulation [34], while “chemical carcinogenesis-reactive oxygen species” and “lipid and atherosclerosis” pathways were involved in oxidative stress responses and lipid metabolism, respectively [15, 32]. GO enrichment analysis further indicated that the key biological processes included transcription factor complex assembly, DNA-binding transcription activator activity, and RNA polymerase II-specific functions, all of which are implicated in modulating inflammation and oxidative stress. Collectively, these results suggest that BHD may exert therapeutic effects in DKD through anti-inflammatory and antioxidant mechanisms.

To validate these predictions, in vivo experiments were performed using high-fat diet combined with low-dose STZ-induced diabetic rats as a model of DKD. Diabetic rats exhibited significant increases in urinary mALB, FBG, BUN, SCr, CHO, and TG, consistent with previous reports [2]. Histopathological examination revealed characteristic renal alterations, including extracellular matrix hyperplasia and basement membrane thickening, confirming successful establishment of the DKD model. Following BHD treatment, levels of CHO, TG, BUN, SCr, and mALB were significantly reduced, comparable to the effects observed with Irbesartan, indicating a protective effect of BHD against renal injury. Notably, BHD did not alter FBG levels, suggesting that its renoprotective effects are independent of glycemic control.

Nrf2 is a critical redox-sensitive transcription factor that regulates the expression of numerous antioxidant genes, including HO-1 and

NQO1. Previous studies have shown that CMFs can activate the Nrf2/HO-1 pathway to mitigate OS and inflammation in DKD. For instance, Yi Shen Pai Du Formula upregulated Nrf2, HO-1, and NQO1, thereby attenuating renal oxidative injury [35]. In our study, BHD treatment significantly increased both total and nuclear Nrf2 expression, indicating activation of the Nrf2/HO-1 pathway. Correspondingly, downstream effectors HO-1 and NQO1 were markedly upregulated at both mRNA and protein levels in BHD-treated rats. Additionally, BHD significantly reduced renal MDA and 8-OHdG levels while restoring SOD activity, demonstrating potent antioxidative effects that likely contribute to renal protection in DKD.

OS is closely intertwined with inflammation, which is a key contributor to DKD pathogenesis [34]. The NF-κB signaling pathway mediates chronic inflammation during DKD progression [32], and its suppression is considered a critical anti-inflammatory mechanism. Proinflammatory cytokines, such as IL-1β and TNF-α, exacerbate renal injury by promoting mesangial cell proliferation, matrix accumulation, endothelial dysfunction, and proteinuria [34]. In this study, renal TNF-α and IL-1β levels were markedly elevated in DM rats but significantly reduced following BHD administration. Consistent with these findings, total and nuclear NF-κB expression was significantly increased in DM rats, whereas BHD treatment effectively suppressed NF-κB activation and nuclear translocation, indicating inhibition of the inflammatory signaling cascade. These results align with previous reports showing that flavonoids such as wogonin can downregulate proinflammatory cytokines and mitigate renal inflammation [36].

Autophagy, a cellular process that degrades damaged cytoplasmic components, plays a critical role in maintaining renal cell homeostasis and mitigating OS-induced injury [37]. While transiently increased in early DKD in response to OS, podocyte autophagy activity becomes impaired during disease progression, contributing to renal damage. Autophagy also modulates inflammatory responses by regulating inflammasome activation through mTOR and AMPK signaling or cytokine production via NF-κB [38-40]. In our study, markers of autophagy were dysregulated in DM rats: P62 was upregulated, whereas Beclin1 and LC3-II/LC3-I were downregulated, reflecting impaired autophagic flux. BHD treatment partially restored autophagy, suggesting a protective role against DKD-associated renal injury.

Renal fibrosis, characterized by ECM deposition including fibronectin and collagen, represents the final stage of DKD progression. OS, inflammation, and autophagy dysfunction are tightly linked to fibrogenesis. TGF-β1 is a key profibrotic cytokine that regulates ECM proteins and modulates inflammatory responses. Immunohistochemical analyses revealed significantly increased renal expression of TGF-β1 and collagen III in DM rats, which was effectively attenuated by BHD or Irbesartan treatment. These findings indicate that BHD exerts antifibrotic effects, likely contributing to its overall renoprotective mechanism in DKD.

Collectively, these results suggest that BHD ameliorates DKD through a multi-targeted mechanism involving activation of Nrf2/HO-1-mediated antioxidative defense, suppression of NF-κB-mediated inflammation, restoration of autophagic flux, and inhibition of renal fibrosis, providing a comprehensive mechanistic basis for its therapeutic efficacy.

Conclusion

In summary, this study elucidated the therapeutic mechanisms of BHD in DKD through an integrated approach combining network pharmacology and experimental validation. Network pharmacology identified key candidate targets and signaling pathways through which BHD may ameliorate DKD progression. Subsequent in vivo experiments confirmed that BHD attenuates renal fibrosis by suppressing oxidative stress and inflammation. Mechanistically, these protective effects are mediated, at least in part, via activation of the Nrf2/HO-1 antioxidative pathway and inhibition of NF-κB-driven inflammatory signaling. Collectively, this integrated analysis provides a comprehensive mechanistic basis and experimental evidence for BHD as a promising multi-target therapeutic strategy for DKD, laying a solid foundation for future preclinical and clinical investigations.

Acknowledgements

This research was supported by the National Natural Science Foundation of China (82274504), Hebei Province Natural Science

Foundation (H2025423034, H2022423320), and Research Foundation of Administration of Traditional Chinese Medicine of Hebei Province (2024102, 2022108).

Disclosure of conflict of interest

None.

Address correspondence to: Yajing Zhang, College of Traditional Chinese Pharmacy, Hebei University of Chinese Medicine, Shijiazhuang, Hebei, China. E-mail: zhangyajing@hebcm.edu.cn; Shengkai Ma, College of Integrative Medicine, Hebei University of Chinese Medicine, Shijiazhuang, Hebei, China. E-mail: mashengkai@hebcm.edu.cn

References

[1] Usuelli V and La Rocca E. Novel therapeutic approaches for diabetic nephropathy and retinopathy. Pharmacol Res 2015; 98: 39-44.

[2] Yang F, Li Y, Guo S, Pan Y, Yan C and Chen Z. Hirudo lyophilized powder ameliorates renal injury in diabetic rats by suppressing oxidative stress and inflammation. Evid Based Complement Alternat Med 2021; 2021: 6657673.

[3] Dounousi E, Duni A, Leivaditis K, Vaios V, Eleftheriadis T and Liakopoulos V. Improvements in the management of diabetic nephropathy. Rev Diabet Stud 2015; 12: 119-33.

[4] Tanase DM, Gosav EM, Anton MI, Floria M, Seritean Isac PN, Hurjui LL, Tarniceriu CC, Costea CF, Ciocoiu M and Rezus C. Oxidative stress and NRF2/KEAP1/ARE pathway in diabetic kidney disease (DKD): new perspectives. Biomolecules 2022; 12: 1227.

[5] Vodošek Hojs N, Bevc S, Ekart R and Hojs R. Oxidative stress markers in chronic kidney disease with emphasis on diabetic nephropathy. Antioxidants (Basel) 2020; 9: 925.

[6] Roumeliotis A, Roumeliotis S, Tsetsos F, Georgitsi M, Georgianos PI, Stamou A, Vasilakou A, Kotsa K, Tsekmekidou X, Paschou P, Panagoutsos S and Liakopoulos V. Oxidative stress genes in diabetes mellitus type 2: association with diabetic kidney disease. Oxid Med Cell Longev 2021; 2021: 2531062.

[7] Sanajou D, Ghorbani Haghjo A, Argani H and Aslani S. AGE-RAGE axis blockade in diabetic nephropathy: current status and future directions. Eur J Pharmacol 2018; 833: 158-164.

[8] Zac-Varghese S and Winocour P. Managing diabetic kidney disease. Br Med Bull 2018; 125: 55-66.

[9] Chen X, Dai W, Li H, Yan Z, Liu Z and He L. Targeted drug delivery strategy: a bridge to the therapy of diabetic kidney disease. Drug Deliv 2023; 30: 2160518.

[10] Covington MB. Traditional Chinese medicine in the treatment of diabetes. Diabetes Spectr 2001; 14: 154-159.

[11] Zhang S, Ma P and Chen Q. The correlation between the level of skin advanced glycation end products in type 2 diabetes mellitus and the stages of diabetic retinopathy and the types of traditional Chinese medicine syndrome. Evid Based Complement Alternat Med 2022; 2022: 5193944.

[12] Zheng XW, Shan CS, Xu QQ, Wang Y, Shi YH, Wang Y and Zheng GQ. Buyang Huanwu Decoction targets SIRT1/VEGF pathway to promote angiogenesis after cerebral ischemia/reperfusion injury. Front Neurosci 2018; 12: 911.

[13] Zhao J, Mo C, Meng LF, Liang CQ, Cao X and Shi W. Efficacy and safety of Buyang Huanwu Decoction for early-stage diabetic nephropathy: a meta-analysis. Zhongguo Zhong Yao Za Zhi 2019; 44: 1660-1667.

[14] Xu J, Bai L, Ma E, Guo Q, Wang Y, Zhang M and Chen Z. Correlativity between blood measures related to blood stasis blocking collaterals and gene expression of angiotensin-converting enzyme of renal cortex in diabetic rats and effect of stasis removing and collaterals dredging. J Tradit Chin Med 2014; 34: 597-603.

[15] Liu B, Song Z, Yu J, Li P, Tang Y and Ge J. The atherosclerosis-ameliorating effects and molecular mechanisms of BuYangHuanWu decoction. Biomed Pharmacother 2020; 123: 109664.

[16] Bao XY, Deng LH, Huang ZJ, Daror AS, Wang ZH, Jin WJ, Zhuang Z, Tong Q, Zheng GQ and Wang Y. Buyang Huanwu Decoction enhances revascularization via Akt/GSK3β/NRF2 pathway in diabetic hindlimb ischemia. Oxid Med Cell Longev 2021; 2021: 1470829.

[17] Khan SA and Lee TKW. Network-pharmacology-based study on active phytochemicals and molecular mechanism of cnidium monnieri in treating hepatocellular carcinoma. Int J Mol Sci 2022; 23: 5400.

[18] Gao R, Zhang X, Zhou Z, Sun J, Tang X, Li J, Zhou X and Shen T. Pharmacological mechanism of Ganlu powder in the treatment of NASH based on network pharmacology and molecular docking. Dis Markers 2022; 2022: 7251450.

[19] Lu J, Yan J, Yan J, Zhang L, Chen M, Chen Q, Cheng L and Li P. Network pharmacology based research into the effect and mechanism of Xijiao Dihuang Decoction against sepsis. Biomed Pharmacother 2020; 122: 109777.

[20] Zeng L, Yang K, Liu H and Zhang G. A network pharmacology approach to investigate the pharmacological effects of Guizhi Fuling Wan on uterine fibroids. Exp Ther Med 2017; 14: 4697-4710.

[21] Skovsø S. Modeling type 2 diabetes in rats using high fat diet and streptozotocin. J Diabetes Investig 2014; 5: 349-58.
[22] Irazabal MV and Torres VE. Reactive oxygen species and redox signaling in chronic kidney disease. Cells 2020; 9: 1342.
[23] Hoesel B and Schmid JA. The complexity of NF-κB signaling in inflammation and cancer. Mol Cancer 2013; 12: 86.
[24] Kaushal GP and Shah SV. Autophagy in acute kidney injury. Kidney Int 2016; 89: 779-91.
[25] Ding Z, Liu S, Wang X, Khaidakov M, Dai Y and Mehta JL. Oxidant stress in mitochondrial DNA damage, autophagy and inflammation in atherosclerosis. Sci Rep 2013; 3: 1077.
[26] Phillips AO. The role of renal proximal tubular cells in diabetic nephropathy. Curr Diab Rep 2003; 3: 491-6.
[27] Li Y, Li L, Zeng O, Liu JM and Yang J. H2S improves renal fibrosis in STZ-induced diabetic rats by ameliorating TGF-β1 expression. Ren Fail 2017; 39: 265-272.
[28] Wen D, Tan RZ, Zhao CY, Li JC, Zhong X, Diao H, Lin X, Duan DD, Fan JM, Xie XS and Wang L. Astragalus mongholicus bunge and panax notoginseng (Burkill) F.H. Chen formula for renal injury in diabetic nephropathy- in vivo and in vitro evidence for autophagy regulation. Front Pharmacol 2020; 11: 732.
[29] Lin X, Lei XQ, Yang JK, Jia J, Zhong X, Tan RZ and Wang L. Astragalus mongholicus bunge and panax notoginseng formula (A&P) improves renal mesangial cell damage in diabetic nephropathy by inhibiting the inflammatory response of infiltrated macrophages. BMC Complement Med Ther 2022; 22: 17.
[30] Guan Y, Quan D, Chen K, Kang L, Yang D, Wu H, Yan M, Wu S, Lv L and Zhang G. Kaempferol inhibits renal fibrosis by suppression of the sonic hedgehog signaling pathway. Phytomedicine 2023; 108: 154246.
[31] Zhou W, Sha Y, Zeng J, Zhang X, Zhang A and Ge X. Computational systems pharmacology, molecular docking and experiments reveal the protective mechanism of Li-Da-Qian mixture in the treatment of glomerulonephritis. J Inflamm Res 2021; 14: 6939-6958.
[32] Ma L, Wu F, Shao Q, Chen G, Xu L and Lu F. Baicalin alleviates oxidative stress and inflammation in diabetic nephropathy via Nrf2 and MAPK signaling pathway. Drug Des Devel Ther 2021; 15: 3207-3221.
[33] Fang J, Wang C, Zheng J and Liu Y. Network pharmacology study of Yishen capsules in the treatment of diabetic nephropathy. PLoS One 2022; 17: e0273498.
[34] Rayego-Mateos S, Morgado-Pascual JL, Opazo-Ríos L, Guerrero-Hue M, García-Caballero C, Vázquez-Carballo C, Mas S, Sanz AB, Herencia C, Mezzano S, Gómez-Guerrero C, Moreno JA and Egido J. Pathogenic pathways and therapeutic approaches targeting inflammation in diabetic nephropathy. Int J Mol Sci 2020; 21: 3798.
[35] Zhang Q, Liu X, Sullivan MA, Shi C and Deng B. Protective effect of Yi Shen Pai Du formula against diabetic kidney injury via inhibition of oxidative stress, inflammation, and epithelial-to-mesenchymal transition in db/db mice. Oxid Med Cell Longev 2021; 2021: 7958021.
[36] Zheng ZC, Zhu W, Lei L, Liu XQ and Wu YG. Wogonin ameliorates renal inflammation and fibrosis by inhibiting NF-κB and TGF-β1/Smad3 signaling pathways in diabetic nephropathy. Drug Des Devel Ther 2020; 14: 4135-4148.
[37] Nam SA, Kim WY, Kim JW, Park SH, Kim HL, Lee MS, Komatsu M, Ha H, Lim JH, Park CW, Yang CW, Kim J and Kim YK. Autophagy attenuates tubulointerstital fibrosis through regulating transforming growth factor-β and NLRP3 inflammasome signaling pathway. Cell Death Dis 2019; 10: 78.
[38] Wang Y, Liu Z, Shu S, Cai J, Tang C and Dong Z. AMPK/mTOR signaling in autophagy regulation during cisplatin-induced acute kidney injury. Front Physiol 2020; 11: 619730.
[39] El-Maadawy WH, Hassan M, Abdou RM, El-Dine RS, Aboushousha T, El-Tanbouly ND and El-Sayed AM. 6-Paradol alleviates diclofenac-induced acute kidney injury via autophagy enhancement-mediated by AMPK/AKT/mTOR and NLRP3 inflammasome pathways. Environ Toxicol Pharmacol 2022; 91: 103817.
[40] Borghi SM, Fattori V, Ruiz-Miyazawa KW, Bertozzi MM, Lourenco-Gonzalez Y, Tatakihara RI, Bussmann AJC, Mazzuco TL, Casagrande R and Verri WA Jr. Pyrrolidine dithiocarbamate inhibits mouse acute kidney injury induced by diclofenac by targeting oxidative damage, cytokines and NF-κB activity. Life Sci 2018; 208: 221-231.

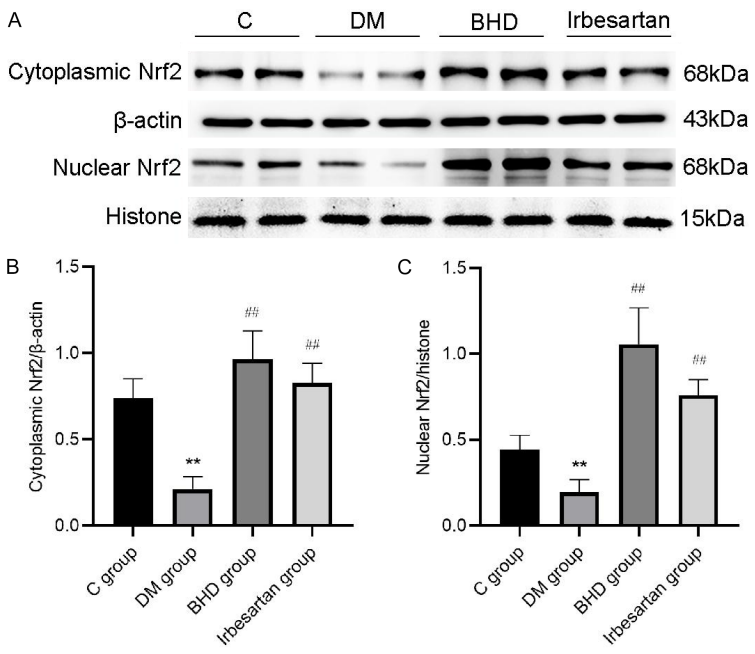

Figure S1. A. The cytoplasmic and nuclear expressions of Nrf2 in each group of rats. B. The quantitative analysis of cytoplasmic Nrf2 expression. C. The quantitative analysis of nuclear Nrf2 expression. Data are presented as means ± SD (n = 3). $^{**}P < 0.01$ vs. C group; $^{\#}P < 0.05$ and $^{\#\#}P < 0.01$ vs. DM group.

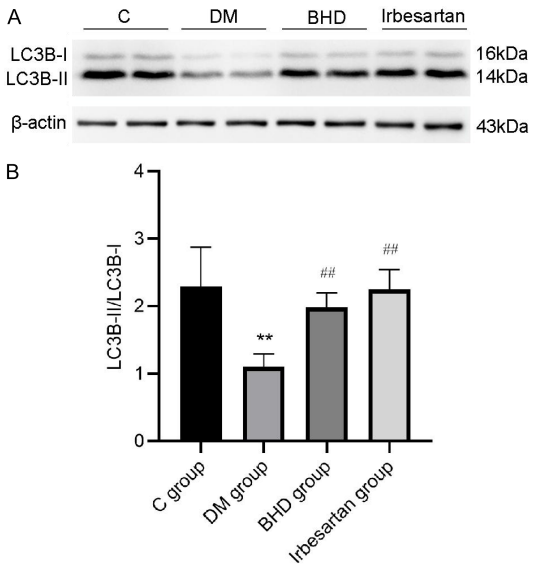

Figure S2. A. The protein expressions of LC3B. B. The quantitative analysis of LC3B-II/LC3B-I protein. Data are presented as means ± SD (n = 3). $^{**}P < 0.01$ vs. C group; $^{\#}P < 0.05$ and $^{\#\#}P < 0.01$ vs. DM group.